7. Oxidation of gold by oxygen-ion sputtering

Up to now, relatively little attention has been paid to oxygen phases obtained by sputtering of gold surfaces with oxygen ions. Nevertheless, the high oxygen loadings obtained in this way, combined with the roughening of the surface due to the sputter deposition, should provide a more 'realistic' model of an oxygen-covered gold catalyst than the 'milder' oxidation methods as, for example, the electron bombardment of physisorbed oxygen described in Chapter 5. Furthermore, oxygen-ion sputtering may also generate oxygen species which have previously only been observed on supported gold particles, but not on gold single crystals. To give an example, oxidation of an Au/SiO_2 catalyst with O_2 or NO_2 led in a TDS experiment to oxygen desorption between 700 K and 1000 K [Ch98], similar to the results reported in this chapter. However, with the previously employed oxidation methods as mentioned in Sections 2.2.1 and 6.1, generally no oxygen desorption above 600 K has been observed in TDS, except for a very weak signal around 900 K after electrochemical oxidation [Pe84]. A study of the behaviour of oxygen implanted into the bulk of the gold crystal, which leads to desorption states at higher temperatures, was therefore a natural continuation of our investigations on chemisorbed oxygen in Chapter 6. Oxygen-ion sputtered Au(110)-(1×2) has not been investigated prior to the work reported here. In the only previous study, Pireaux et al. sputtered Au(111) with oxygen ions for up to fifteen minutes by applying an ion current of 1 mA (at 500 eV ion energy), and obtained surfaces of dark blue colour due to relatively thick layers of gold oxide (Au_2O_3) [Pi84].

Sputtering of the gold (110) surface with oxygen ions (O^+/O_2^+) leads to the simultaneous occupation of different adsorption sites on the surface and in the bulk. In order to distinguish between surface and bulk species it proves useful to combine methods of high surface sensitivity with those that detect all deposited particles, both on the surface and in the surface-near bulk. A method that monitors every adsorbate species is TDS, provided the desorption temperature of the respective species is reached. In contrast, titration with a reactive gas, here CO, can be very surface sensitive, unless the volume species is mobile enough to segregate to the surface. The work function change, on the other hand, is usually dominated by adsorbed particles on the surface and – less pronounced – in the subsurface range. Accordingly, the surface-analytical tools employed in this chapter include thermal desorption spectroscopy (TDS), work function measurements ($\Delta\varphi$), reaction with carbon monoxide, and, supplementing structural information, low-energy electron diffraction (LEED).

In all oxygen-ion sputtering experiments, the oxygen background pressure was $\approx 1\times10^{-4}$ mbar. Ion energies between 1.0 keV and 5.0 keV and ion current densities between 1.5 µA and 3.0 µA (at the sample) were employed. The ion source (sputter gun)

was supplied by backfilling the chamber with oxygen[1]. During oxygen-ion sputtering, the sample temperature was always 300 ± 10 K.

Heating of the sample to 1000 K during TD and $\Delta\varphi$ measurements led to an irreversible roughening of the gold (110) surface (cf. Section 2.1 and Ref. [Ro91]). To regain a well-defined sample, the surface was Ar-ion sputtered for one hour and annealed at 640 K for five minutes subsequent to each TD measurement.

In the following, the term 'coverage' with its units [cm^{-2}] and [monolayer (ML)] is used in the sense of 'coverage equivalent' to describe the total amount of oxygen atoms on the surface *and* in the bulk. This amount is related to the surface area or to the number of gold atoms per area of the ideal Au(110)-(1×2) surface without presupposing that the oxygen atoms are actually located *on* the surface. The monolayer [ML] is defined as one oxygen atom (on the surface or in the bulk) per surface gold atom, equivalent to four atoms in the 2.89 Å × 8.16 Å unit cell or to 1.696×10^{15} oxygen atoms per cm^2.

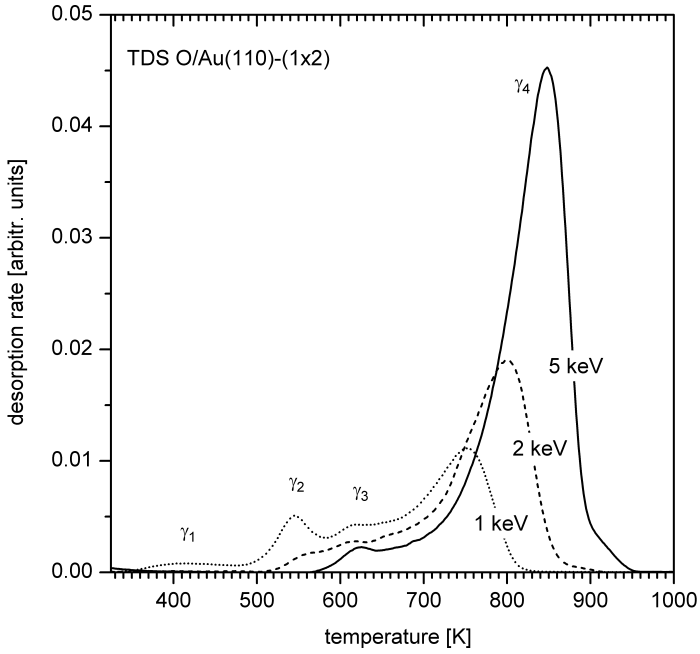

Fig. 7.1: Set of thermal desorption spectra of oxygen on Au(110)-(1×2), measured after 10 minutes oxygen-ion sputtering with the indicated ion energies. The spectra were taken with a heating rate of 1.0 K/s; the detected mass was m/z = 32.

[1] Oxygen gas 4.8 (> 99.998% O_2), Messer Griesheim, Germany.

7.1. Thermal desorption spectra of sputter-deposited oxygen

7.1.1. Variation of the oxygen ion energy

The clean Au(110)-(1×2) surface was sputtered with oxygen ions of three different energies, viz., 1.0 keV, 2.0 keV, and 5.0 keV with ion current densities of 1.5 $\mu A/cm^2$, 2.0 $\mu A/cm^2$, and 3.0 $\mu A/cm^2$, respectively. The sputtering was always performed for 10 minutes using normal ion incidence.

After sputtering with ions of a given energy, the resulting adsorbate phase was investigated with TDS. Fig. 7.1 shows thermal desorption traces (m/z = 32), taken with a heating rate of 1.0 K/s for the three ion energies mentioned above. Curve (a), corresponding to the lowest ion energy (1.0 keV), exhibits four desorption states γ_1 to γ_4 with maximum desorption (T_{max}) at 415 K, 545 K, 620 K, and 750 K, respectively. No oxygen desorption occurred above 1000 K. The peaks γ_2 and γ_1 resemble closely the desorption states of chemisorbed oxygen and gold oxide, respectively, on Au(110)-(1x2). In contrast, the peaks γ_3 and γ_4 were observed for the first time and can be assigned to subsurface and/or bulk oxygen species.

If the ion energy is increased to 2.0 keV (curve b), the low-temperature peaks γ_1 - γ_3 lose intensity, while γ_4 grows and shifts to higher temperatures (T_{max} = 800 K), a tendency which continues for a further increase of the ion energy: at 5.0 keV (curve c), γ_1 and γ_2 have almost vanished, and γ_4 has grown further, along with a shift of the maximum to 850 K. This observation likely reflects the fact that high-energy ions are unable to dissipate their kinetic energy immediately upon impact. Rather, they penetrate the surface region and reach sites deeper inside the volume. Therefore, almost no chemisorbed oxygen or surface gold oxide is formed at high ion energies (5.0 keV), and the peaks γ_1 and γ_2 disappear. Alternatively, the increased sputtering rates at high ion energies could lead to the removal of γ_1 and γ_2. This explanation is also consistent with the assignment of γ_1 and γ_2 to on-surface oxygen. The γ_4 peak exhibits a significant shift to higher temperatures as the ion energy increases; the leading edges of the peaks even cross. The high T_{max}-values suggest relatively large desorption activation energies, which may be interpreted in several ways. One possibility is that 'trapping centres' possessing a high local binding energy may accompany defect sites formed in the surface-near region during bombardment. However, the high-temperature shift of γ_4 with increasing ion energy also indicates an increase of the desorption energy with the penetration depth of the ions. At the kinetic energies employed in our experiments the average penetration depth of the ions certainly exceeds several Å. At these depths below the surface the influence of the asymmetries in the surface region are expected to be negligible. It is therefore unlikely that oxygen is located within the upper atomic layers of the crystal and that the high desorption temperatures originate from a large activation energy of sites in the damaged surface region. More likely, thermally activated diffusion controls the transport of O atoms trapped in bulk sites to the surface. In this case, the desorption temperature would not only be controlled by the bulk binding energy of the oxygen

atoms. For a given temperature, diffusion-limited desorption of oxygen atoms from the deep bulk should always occur *later in time* than desorption from sites closer to the surface. In the TD experiment, this temporal shift of the desorption events becomes apparent as a higher desorption temperature.

We have obtained evidence for partial atomic desorption of the states γ_1, γ_2, and γ_3 (Fig. 7.2). The oxygen phase used for this experiment was prepared by 10 minutes of sputtering with oxygen ions (kinetic energy: 2.0 keV) at a sample current density of 2.0 $\mu A/cm^2$. If the oxygen were to desorb exclusively as O_2, then the two curves in Fig. 7.2 representing mass 16 and mass 32 intensity should be identical within the noise. The significant deviations between 350 K and 750 K clearly reveal an excess of O^+ ions in this region. This observation suggests strongly that the states γ_1 - γ_3 desorb partially as atomic oxygen, in contrast to γ_4. (An alternative explanation could be that desorption of electronically or vibrationally excited oxygen molecules might allow stronger fragmentation to atomic oxygen during ionisation in ion source of the mass spectrometer.) Contributions due to desorption of co-adsorbed water or carbon dioxide, which would also lead to a higher m/z = 16 intensity, were excluded by simultaneous monitoring of ions with m/z = 18 and 44.

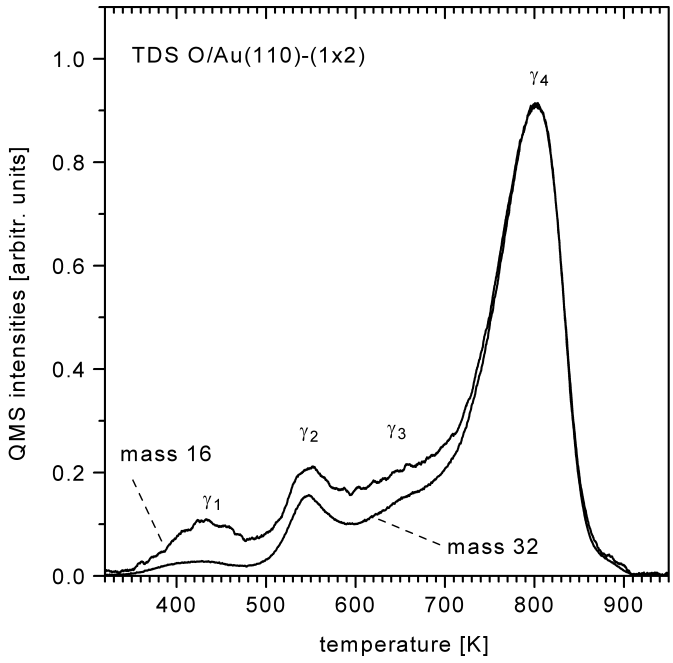

Fig. 7.2: Oxygen thermal desorption spectrum with simultaneous detection of (a) m/z = 16 and (b) m/z = 32. Curve (a) was multiplied by a factor 12 taking into account the mass 16 to mass 32 QMS intensity ratio of 1:12 for pure O_2 supplied directly to the mass spectrometer (this ratio was constant throughout the relevant pressure range from 10^{-9} mbar to 10^{-5} mbar). The deviation of the curves shows atomic desorption for the peaks γ_1 - γ_3. Details about the preparation of the oxygen phase in the text.

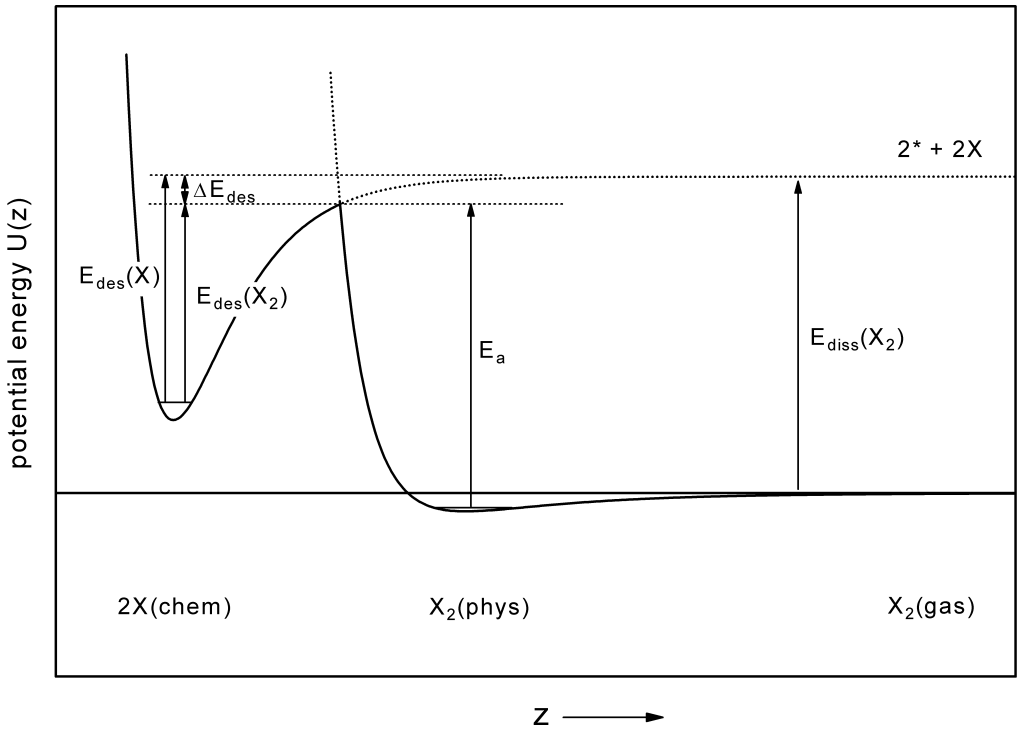

Fig. 7.3: Schematic energy diagram for a highly activated dissociative adsorption of a diatomic molecule X_2. The chemisorbed species X(chem) is assumed to be metastable (endothermic) relative to the elements (as it is the case for O/Au).

The atomic desorption can be interpreted in the following way: dissociative chemisorption of oxygen on gold is highly activated, i.e., the oxygen molecules have to be almost completely dissociated in order to become adsorbed. According to the principle of microscopic reversibility [To24], desorption proceeds along the same path as adsorption – in the reverse direction. Therefore, atomic desorption should be almost as likely as the desorption of molecules. A schematic energy diagram for such a system is displayed in Fig. 7.3. It illustrates that atomic desorption becomes more and more efficient if the chemisorption activation energy approaches the gas-phase dissociation energy of the molecule. From the observed O/O_2 ratio we can estimate a the difference of the activation energies of atomic and molecular desorption, ΔE_{des}, using Eq. 4.1. Applying a temperature of 430 K (γ_1 state), we obtain $\Delta E_{des} \approx 15$ kJ/mol. With the activation energy for molecular desorption, 140 kJ/mol (see Section 6.1), we are able to estimate the desorption energy for one atom (155 kJ/mol) and, trivially, for two atoms (310 kJ/mol). The latter value fixes the energy of chemisorbed oxygen and allows an estimate for the activation energy of dissociative chemisorption (≈339 kJ/mol). Thus, we now are able to report a complete energy diagram of the oxygen/gold system, which is displayed in Fig. 7.4. Unfortunately, there are still contradictions and unsolved problems connected with our interpretation. First, atomic desorption should also be observed for chemisorbed oxygen produced by electron bombardment physisorbed O_2. This, however, is not the case. Second, the O/O_2 ratio should go up with increasing temperature because

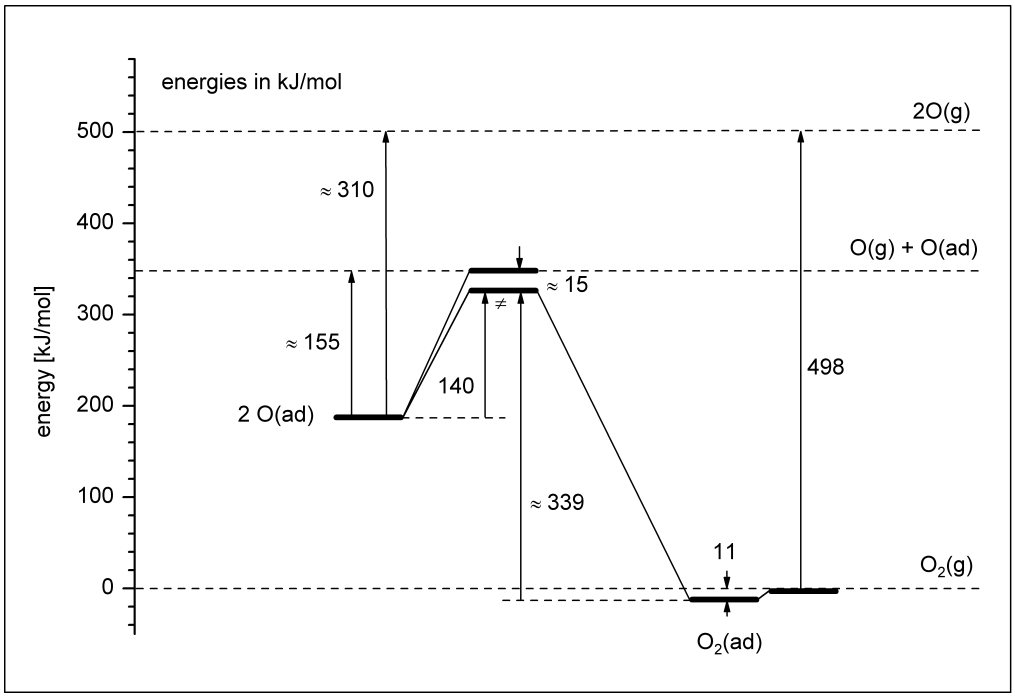

Fig. 7.4: Energy diagram of the oxygen-gold adsorption system. See the text for further explanations.

of the diminishing influence of the exponential term. There is also no sign of this effect. Moreover, the high-temperature γ_4 state shows no atomic desorption. At present, we are not able to give a proper explanation for these observations, which makes the energy diagram in Fig. 7.4 somewhat speculative.

7.1.2. Variation of the exposure time

In a second type of experiment, the exposure time to oxygen ions (sputtering time) was systematically varied between one minute and 20 minutes at a constant ion energy of 2.0 keV. This energy is sufficiently low to provide occupation of the γ_1 and γ_2 adsorption sites on the surface. During sputtering, a current density of 2.0 $\mu A/cm^2$ was adjusted. Thereafter, the thermal desorption experiment was performed with a heating rate of 1.0 K/s by detection of mass 32. A representative selection of the resulting desorption traces is displayed in Fig. 7.5. Short sputtering for one minute populated the γ_3 and γ_4 states (curve a). For prolonged sputtering times, however, all peaks γ_1 to γ_4 appeared simultaneously (curves b-e). We note that the maxima of the γ_2 state shift to lower temperatures with increasing oxygen loading (from 570 to 540 K); a reverse shift is observed for the γ_4 state (from ≈ 680 to 830 K). The low-temperature shift of γ_2 is indicative of a desorption order > 1 and suggests that γ_2 originates from chemisorbed oxygen atoms. The rate-limiting step for molecular desorption is then the recombination of individual oxygen atoms.

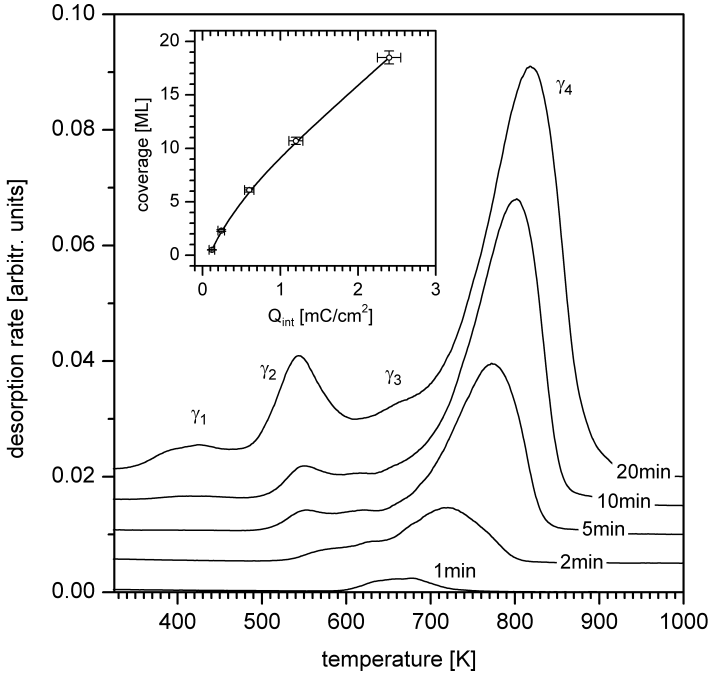

Fig. 7.5: Set of oxygen thermal desorption spectra taken after oxygen-ion sputtering for the indicated periods of time. The spectra were measured with a heating rate of 1.0 K/s by detection of m/z = 32. Inset: Plot of the oxygen coverage vs. the integrated charge flux per unit sample area (Q_{int}). Q_{int} is the product of sample current density and sputtering time. Monolayer coverage corresponds to one oxygen atom per surface gold atom (1.696×10^{15} cm^{-2}).

In contrast, the high-temperature shift of γ_4 suggests a desorption order < 1 for the bulk oxygen species. A desorption order < 1 often reflects desorption from a reservoir of particles, e.g., multilayers, islands, etc., if the desorption rate is additionally limited by geometrical factors. Such factors include the surface area in the case of multilayer desorption and the island perimeter in the case of island desorption. In the present case, the reservoir may consist of oxygen atoms absorbed in the bulk, and the limiting geometrical factor is probably the number of diffusion/segregation channels available for the O atoms at the surface.

Integration of the TD spectra in Fig. 7.5 provides absolute oxygen coverages by the method described in Section 4.1.6. Relative coverages were obtained by dividing the absolute coverages by the number of surface gold atoms per area (1.696×10^{15} cm^{-2}). In the inset of Fig. 7.5, these relative coverages are plotted vs. the *integrated charge flux per unit sample area* Q_{int}, which is the product of sample current density and sputtering time. Q_{int} is proportional to the total number of oxygen ions that are neutralized on the surface, at least for a fixed ion energy. However, we do not attempt here to establish a relationship between Q_{int} and the number of ions, since other processes, mainly secondary electron emission, may interfere. This problem is dealt with in more detail in Section 7.5. We note that the oxygen coverage depends almost linearly on Q_{int}, except for low coverages (< 2 ML). Due to the large number of vacant sites, the concentration of oxygen atoms in

the bulk remains very small under the conditions of the experiment ($\Theta_0 \leq 18.5$ ML). It is therefore not surprising that no saturation behaviour is observed.

7.1.3. Activation parameters for desorption determined by heating rate variation

In order to determine the activation parameters of desorption we varied the heating rate of the TDS experiment at constant oxygen coverage. We prepared the oxygen adsorbate phases by sputtering the sample for 10 minutes with oxygen ions of 1.0 keV energy at a sample current density of 1.5 μA/cm^2. This treatment led to a coverage of 7.8×10^{15} oxygen atoms per cm^2, equivalent to 4.6 ML. Fig. 7.6 displays thermal desorption traces for four different heating rates between 0.05 K/s and 7.6 K/s. With increasing heating rate, the peaks γ_1, γ_2, and γ_4 shift to higher temperatures, a behaviour that is consistent with the prediction of the Polanyi-Wigner equation (Eq. 4.1). Remarkably, γ_3 does not shift with the heating rate, a phenomenon that is more closely inspected in Section 7.5.

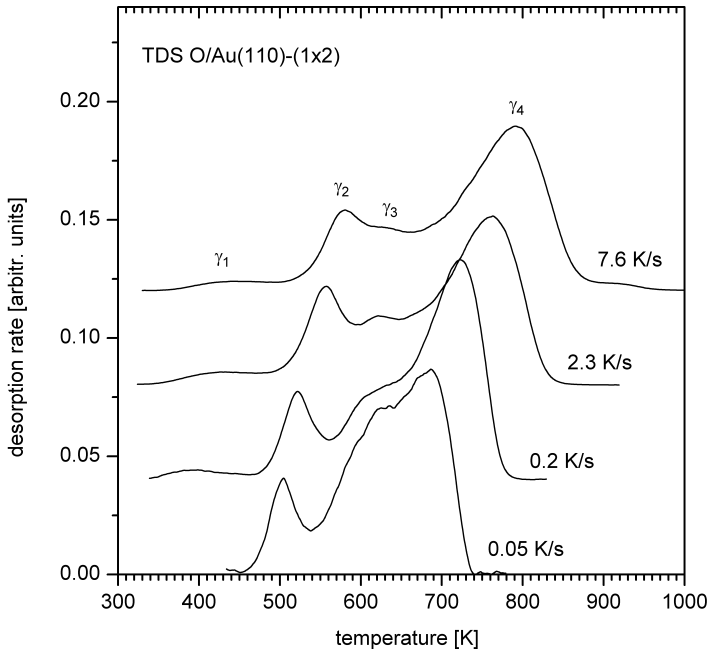

Fig. 7.6: Set of oxygen thermal desorption spectra (detected mass: m/z = 32) for the same initial oxygen coverage (7.8×10^{15} oxygen atoms per cm^2, equivalent to 4.6 ML), taken with different heating rates as indicated. The spectra were normalized with respect to the integrated intensity. Due to the low particle flux at small heating rates, the weak γ_1 peak is suppressed in spectrum (a). See text for the further details.

The evaluation of the kinetic and energetic parameters of the desorption process, i.e., the desorption activation energy, E_{des}, and the frequency factor, ν_n, from a TDS experiment with variable heating rate is provided by Eq. 4.11. Here, we assume somewhat arbitrary n = 1 (but see below). According to Eq. 4.11, plots of $\ln(\widetilde{T}_{max}^2 / \widetilde{\beta})$ vs. $1/T_{max}$ as shown in Fig. 7.7 are linear if the desorption behaviour is consistent with the Polanyi-Wigner equation (Eq. 4.1). Furthermore, from the slope and intercept of the best fit, the desorption energies E_{des} and the frequency factors ν_1 can be determined. The values are presented in Table 7.1. E_{des} values obtained with the Redhead formula (Eq. 4.12) (using a frequency factor of 1×10^{13} s^{-1}) are included for comparison. The Redhead values are in good agreement (within ± 10 %) with those derived from the heating rate variation because the actual frequency factors are indeed close to the arbitrarily chosen value of 1×10^{13} s^{-1}.

All frequency factors for the desorption states γ_1 - γ_4 are close to the universal frequency factor kT/h, which is 8×10^{12} s^{-1} - 1.7×10^{13} s^{-1} between 400 K and 800 K. According to transition state theory, a frequency factor of ≈ kT/h is consistent with a mobile adsorbate with two translational degrees of freedom, while values up to 100 times higher are typical of immobile adsorbates (see, for example, [Dr74]). We conclude that all observed oxygen phases are mobile at their respective desorption temperatures. This conclusion does not apply to the γ_4 state if the desorption of this state is diffusion-controlled. (In this case, the parameters would represent the activation energy and the frequency factor for the diffusion of oxygen atoms in gold.)

In our TDS analysis we assumed a desorption order of n = 1. If the actual order deviates from 1, an error in ν_1 (but not in E_{des}) will occur due to the term proportional to $\ln\Theta_{max}$ in Eq. 4.11. This error is small (< 5 %) as long as $0.5 < \Theta_{max} < 5$ ML. The actual coverages at the desorption maxima (Θ_{max}) remain within these limits.

7.2. Reaction with carbon monoxide

It will be shown in Chapter 11 that chemisorbed oxygen atoms and on-surface gold oxide react at 300 K vigorously with carbon monoxide (CO) forming CO_2, which desorbs immediately. A CO dosage of ≈ 500 L proved to be sufficient for the complete removal of chemisorbed oxygen and gold oxide with a combined coverage of ≈ 2 monolayer equivalents. It is, however, unlikely that implanted oxygen atoms located deep inside the Au bulk will be able to react with CO at 300 K, since the oxygen atoms are not sufficiently mobile in the metal lattice to allow the reactants to come into contact. The low mobility of the bulk oxygen atoms at room temperature follows from two observations: First, chemisorbed oxygen and gold oxide produced on the gold surface completely desorb below 600 K, without competing bulk diffusion (Section 6.1). Second, we found that the desorption of γ_4 is likely to be diffusion-controlled (vide supra).

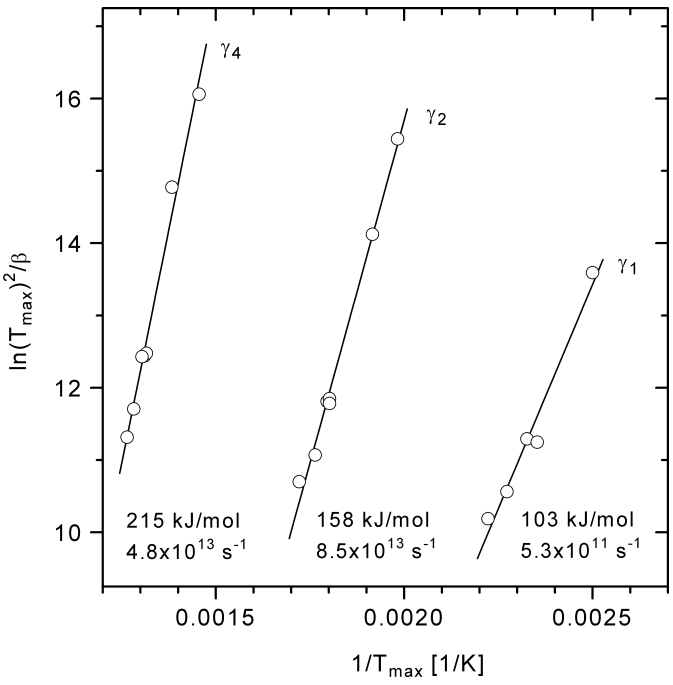

Fig. 7.7: Plot of $\ln(\tilde{T}_{max}^2/\tilde{\beta})$ vs. $1/T_{max}$ for the desorption maxima γ_1, γ_2, and γ_4 of the TD spectra in Fig. 7.6 (and further TD spectra). The indicated desorption activation parameters were determined from the slopes and the intercepts of the best linear fits using Eq. 4.11.

	Heating rate variation		**Redhead**
	E_{des} [kJ/mol]	ν_1 [s^{-1}]	E_{des} [kJ/mol]
γ_1	103	5.3×10^{11}	113
γ_2	158	8.5×10^{13}	148
γ_3	--	--	165
γ_4	215	4.8×10^{13}	204

Table 7.1: Desorption activation energy E_{des} and frequency factor ν_1 as derived from a heating rate variation. For comparison, E_{des} values obtained by Redhead analysis (Ref. [Re62] and Section 4.1.3) are included.

Therefore, TDS proves that the oxygen atoms become sufficiently mobile (on the time scale of our experiments) only beyond 650 K. The diffusion rate at 300 K must be negligibly small since it depends exponentially on temperature. We expect that an excess of CO will completely remove all oxygen that is located at the surface, whereas bulk oxygen resists the CO exposure and can be detected in a subsequent TDS experiment. In other words, CO titration allows a clear distinction between surface and bulk oxygen species. These considerations can be applied to the thermal desorption spectra in Fig. 7.8. Curve (a) was measured directly after a 10 minutes oxygen sputtering (ion energy = 1.0 keV, current density = 1.5 μA/cm^2). The other curve (b) was obtained after a likewise prepared oxygen phase had been treated at 300 K with 8000 L carbon monoxide[2] (800 s × 1.3×10^{-5} mbar) prior to the TDS experiment. In curve (b), the peaks γ_1 and γ_2 were almost entirely eliminated by the CO treatment, whereas γ_3 shows a reduced intensity. The γ_4 peak is not affected at all. These observations confirm that the γ_1 and γ_2 states arise from oxygen species located on the surface, whereas the peak γ_4 is due to oxygen placed in the bulk of the crystal. The origin of the peak γ_3 is somewhat unclear. Considering its intermediate reactivity, we may associate it with an oxygen species located in the surface-near region.

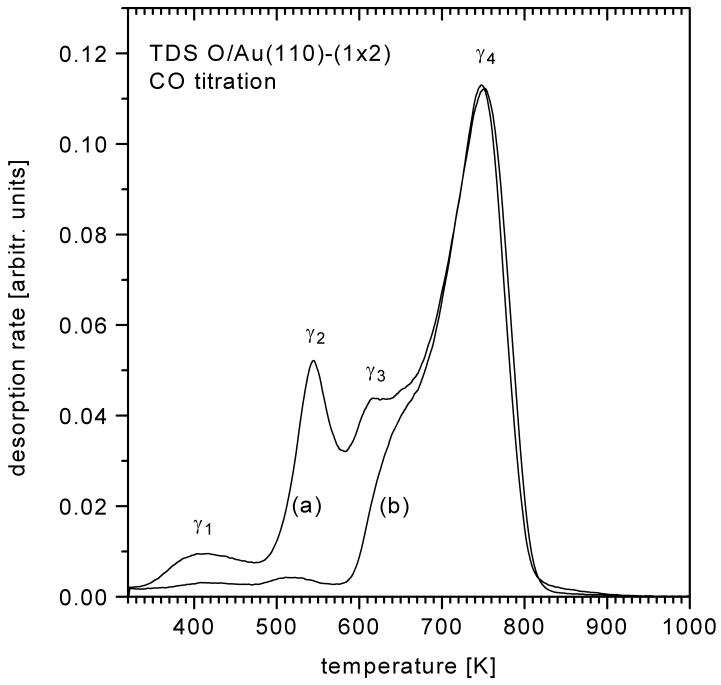

Fig. 7.8: Oxygen thermal desorption spectra, taken with a heating rate of 1.0 K/s by detection of mass 32. In either case, the sample was sputtered for 10 minutes with oxygen ions of an energy of 1.0 keV. (a) TDS without prior CO treatment. (b) Sample treated with 8000 L (800 s × 1.3×10^{-5} mbar) CO prior to the TDS measurement.

[2] CO gas 3.7 (> 99.97 %), Linde, Germany.

7.3. Work function change (Δφ)

From previous studies on oxygen phases produced by electron bombardment of physisorbed oxygen, we know that chemisorbed atomic oxygen leads to a work function increase of + 1.0 eV at monolayer coverage, whereas the surface gold oxide has only little influence on φ (see Section 6.5). In Fig. 7.9, the work function change due to sputtering and subsequent heating of the sample is displayed as a function of temperature. The first point of the curve ($\Delta\varphi \equiv 0$) refers to the clean surface. 20 minutes oxygen sputtering (ion energy = 2.0 keV, sample current density = 2.0 μA/cm^2) causes an initial jump in Δφ of 0.16 eV. For sputtering, the same conditions were applied as in the case of spectrum (e) of Fig. 7.5, resulting in a coverage of 3.1×10^{16} oxygen atoms per cm^2 or 18.5 ML equivalents.

Notably, thermal desorption of γ_1 (performed with an effective heating rate of ≈ 1 K/s) is accompanied by a Δφ increase until a maximum of 0.41 eV is reached at 500 K. If we assume that φ increases really due to the *desorption* of γ_1, then this would suggest to assign this state to subsurface oxygen, which has frequently been reported to lower the work function (see, for example, Refs. [Ga77, Ho79a, Mi80, He89, Bo96, Bö99, Ki01]). Subsurface oxygen atoms could also segregate to unoccupied adsorption sites on the surface and thereby cause or enhance the work function increase.

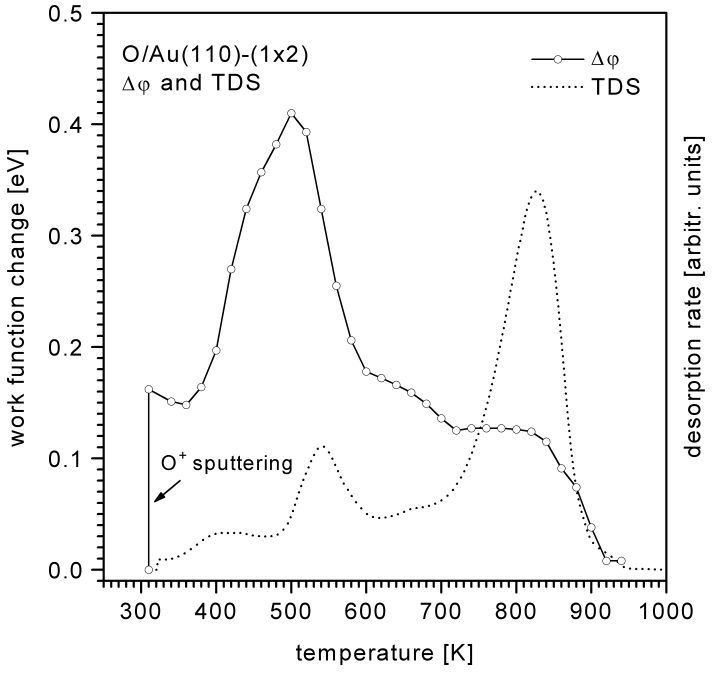

Fig. 7.9: Work function change vs. temperature for sputtered oxygen on Au(110)-(1×2). The oxygen phase was prepared by 20 minutes sputtering with oxygen ions of an energy of 2.0 keV (sample current density 2.0 μA/cm^2). The same treatment as for spectrum (e) in Fig. 7.5 (here included as dotted line) was applied. See text for the further details.

Alternatively, dissolution of islands of chemisorbed oxygen atoms (or even crystallites of surface gold oxide), leading to a reduction of depolarization effects, could also explain the $\Delta\varphi$ curve in this temperature range without attributing γ_1 to subsurface oxygen.

Desorption of the γ_2 state takes place at temperatures above 500 K, resulting in a work function decrease until a value of 0.18 eV is reached around 600 K. The positive work function change caused by γ_2 is consistent with an assignment to negatively polarized on-surface oxygen atoms. We note that the $\Delta\varphi$ values measured (i) directly after sputtering and (ii) after heating to 600 K are very similar (0.16 eV and 0.18 eV, respectively). This could mean that immediately after sputtering the surface is nearly free of chemisorbed oxygen. This conclusion is also consistent with He-I UV photoelectron spectra taken after the oxygen sputtering, which do not show any oxygen induced-features in the valence band region. However, the low total $\Delta\varphi$ value measured directly after sputtering could also result from a partial compensation of the opposite effects of γ_1 ($\Delta\varphi < 0$ for subsurface oxygen) and γ_2 ($\Delta\varphi > 0$ for on-surface oxygen) on the work function, as discussed above.

Desorption of the γ_3 state between 600 K and 700 K is accompanied by a further work function decrease of ≈ 40 meV. The constant value ($\Delta\varphi \approx 0.13$ eV) between 700 K and 820 K obviously reflects the remaining bulk oxygen species γ_4, since $\Delta\varphi$ decreases rapidly as γ_4 desorbs above 820 K. Finally, for temperatures beyond 920 K, the initial work function value of the clean Au(110)-(1×2) surface is nearly restored. The positive $\Delta\varphi$ values for γ_3 and γ_4 exclude the assignment of these states to subsurface oxygen, which generally leads to a work function decrease, as mentioned above. At present, we are not able to explain how a species as γ_4, which must – by all other evidence – be regarded as bulk oxygen, can influence the work function at all. The possible existence of a strongly bound on-surface species (as observed on the oxygen-silver system), which may cause the work function change, will be discussed in Section 7.5.

7.4. Low-energy electron diffraction (LEED)

It has previously been shown that chemisorption of O atoms on gold single-crystal surfaces leads to a complete suppression of the substrate LEED spots at monolayer coverage, i.e., to a disruption of the long range order of the substrate lattice (see [Sa86, Sa98] and Section 6.3). Annealing experiments at elevated temperatures, but below the desorption temperature of chemisorbed O, proved ineffective to restore substrate or to induce adsorbate order. Rather, removal of the chemisorbed oxygen by thermal desorption, sputtering, or reaction with CO was necessary in order to regain substrate long-range order. Therefore, we may regard permanent suppression of the substrate spots as an indication for oxygen chemisorption.

Furthermore, Au(111) surfaces have been reported to undergo restructuring when exposed to O_2 at atmospheric pressure and high temperature (1070 K) for prolonged periods of time (up to 24 h). Scanning tunneling microscopy (STM) investigations revealed a $(\sqrt{3} \times \sqrt{3})\,\mathrm{R30°}$ surface structure combined with a long-range ordered

hexagonal superstructure [Hu95], which was interpreted as a moiré type pattern [Ch96]. Later, also a 'modified herringbone pattern' was observed [Hu96]. The results were confirmed by reflection electron microscopy (REM) and reflection high energy electron diffraction (RHEED) [Uc98]. Interpretation of these observations was dominated by a comparison with Ag(111). It had previously been reported that a similar high-pressure, high-temperature oxygen treatment of the Ag(111) surface leads to the formation of the strongly chemisorbed 'surface-embedded' O_γ species (see Section 7.5ii for a detailed comparison with the O/Ag system), accompanied by a similar restructuring as observed on Au(111) [Ba93]. Therefore, the restructuring of the Au(111) surface has been attributed to strongly chemisorbed atomic oxygen [Hu95, Ch96, Hu96, Uc98], although no *chemical* evidence for the existence of such a species has been delivered.

LEED investigations of chemisorbed oxygen, produced by sputter deposition, were carried out for several O^+/O_2^+ ion energies (1 - 5 keV). Generally, the ion energy proved to be of little influence within this range. As representative examples, Figs. 7.10B and 7.10C show LEED photographs taken after bombardment with oxygen ions (2 μA at 2 keV) for increasing periodes of time, viz., 10 and 20 minutes. Exactly the same sputtering conditions as for the TD spectra (d) and (e) in Fig. 7.5 were applied. As expected, the substrate order is increasingly reduced due to the ion bombardment. However, even high O loading (18.5 ML for Fig. 7.10C, 3.7 ML contained in γ_1 and γ_2) does not lead to a *complete* disruption of the long-range substrate order, in contrast to previous observations on chemisorbed O at monolayer coverage, produced by thermal predissociation of O_2 [Sa86], dosing of O_3 [Sa98], or electron bombardment of physisorbed O_2 (Section 6.3). We conclude that no closed adlayer of chemisorbed oxygen is formed. Rather, the O atoms are distributed on the surface, in the subsurface range, and in the surface-near bulk.

Furthermore, we compared the results of sputtering with inert gas ions (Ar^+) and with oxygen ions for the same integrated charge flux per unit sample area of Q_{int} = 2.4 mC/cm^2. Both treatments had similar effects on the substate LEED picture, as demonstrated by Figs. 7.10C and 7.10G. However, differences became obvious during the annealing process: The long-range order of the Ar^+-sputtered surface was completely restored by heating to 500 K (Fig. 7.10I), in contrast to the oxygen-sputtered surface, where complete desorption of the on-surface species γ_2, achieved by heating to 650 K, was necessary (Figs. 7.10D - 7.10F). In the case of damage by Ar^+ sputtering, annealing occurred first, below 400 K, in the $[\bar{1}\,10]$ direction (Fig. 7.10H), and then, around 500 K, in the $[00\,\bar{1}\,]$ direction (Fig. 7.10I). In contrast, the desorption temperature of the on-surface species γ_2 is sufficiently high that, after oxygen desorption, annealing occurs instantaneously in both directions. The fact that the surface long-range order is *not* disturbed by the presence of γ_4 oxygen is a further support for the assignment of this species to bulk oxygen. Under the conditions of our experiment, we could not observe any oxygen-induced restructuring due to a strongly chemisorbed atomic oxygen species as it has been reported for Au(111) (*vide supra*).

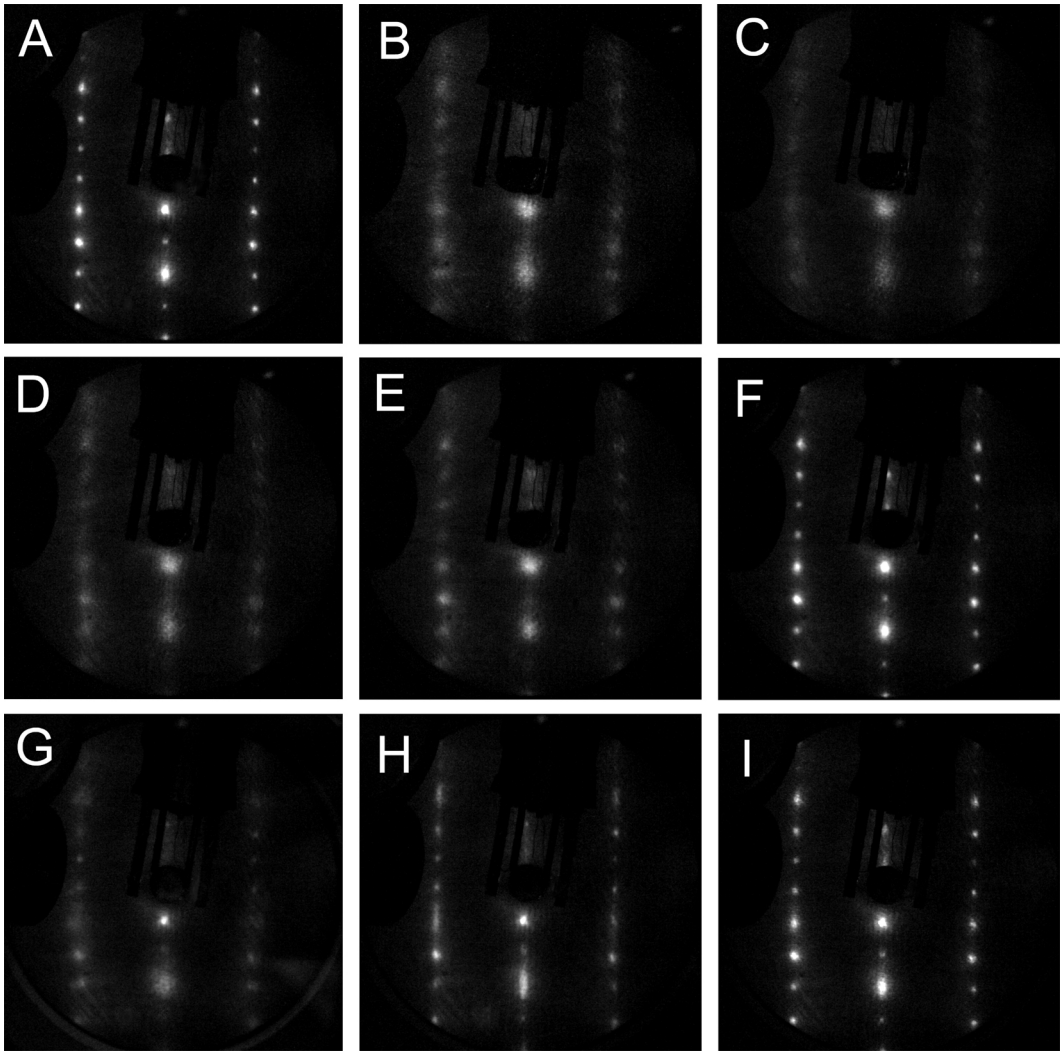

Fig. 7.10: LEED patterns of clean, O^+-, and Ar^+-sputtered Au(110)-(1×2). The photographs were taken at 300 K using an incident beam energy of 122 eV. For sputtering, an ion current of 2.0 μA at 2.0 keV ion energy was applied in all cases. (A) Clean Au(110)-(1×2) surface. O^+ sputtering: (B) for 10 min (1.2 mC/cm^2), (C) for 20 min (2.4 mC/cm^2). Heating subsequent to O^+ sputtering: (D) to 400 K, (E) 500 K, (F) 650 K. Comparison with Ar^+ sputtering: (G) 20 min Ar^+ sputtering (2.0 keV, 2.0 μA, 2.4 mC/cm^2), (H) after heating to 400 K, (I) after heating to 500 K.

7.5. Discussion

(i) COMPARISON WITH OXYGEN-ION SPUTTERED AU(111) – Pireaux et al. [Pi84] sputtered a gold (111) sample with oxygen using a sample current of 1 mA at an ion energy of 500 eV. After it had been sputtered for 15 minutes, the gold crystal exhibited a dark blue colour due to gold oxide layers (Au_2O_3). By comparison with the conditions and results of our experiment, we conclude that the authors produced relatively thick oxide layers of ≈ 10^3 Å. In XPS, they observed Au $4f_{7/2}$ peaks at 84.0 eV (metal) and 85.9 eV (oxide), while two O 1s peaks appeared at 530.2 eV and 535.7 eV. The 85.9 eV peak lost intensity above 390 K (a temperature at which we observe rapid desorption of γ_1) and disappeared at 590 K (at which temperature the desorption of

chemisorbed oxygen on this surface is complete [Sa98]). However, a residual 530 eV peak of oxygen was still detected at this temperature. Unfortunately, the authors did not further examine the temperature dependence of this state, which we associate with a bulk oxygen species similar to our γ_4 state.

(ii) COMPARISON WITH DISSOLVED OXYGEN IN SILVER – From its chemical and structural behaviour gold resembles silver in many respects. Therefore it is useful to compare our findings with results obtained for the O/Ag system. Numerous reports exist on oxygen/silver adsorption phenomena, and we do not regard it useful to cite all the literature. Rather, we refer the reader to a recent article on that topic, which gives an overview of the respective literature [Li02].

Adsorption of oxygen on silver surfaces under UHV conditions and at sample temperatures below 500 K was investigated by many authors (see, e.g., [Li02, Re91] for references). All thermal desorption studies reported a single desorption peak at 595 ± 25 K, which was attributed to adsorbed atomic oxygen. In contrast, and much more relevant in our context, three different atomic oxygen species have been observed after exposure of silver to oxygen at atmospheric pressure above 600 K [Re91a, Ba93, Ba93a, Sc94, Sc95, Ba96, He96]. These species have been assigned to on-surface oxygen (O_α), bulk-dissolved oxygen (O_β), and 'surface-embedded' oxygen (O_γ), and they desorb from a polycrystalline Ag sample at ≤ 600 K (O_α), 600 K - 900 K (O_β), and ≈ 900 K (O_γ) [Re91a, Ba93a, Sc94, He96]. As already mentioned, the formation of O_γ is accompanied by a substantial restructuring of the Ag surface [Ba93, He96]. Rehren et al. [Re91] reported TD spectra for high-temperature and high-pressure oxygen adsorption on silver. They observed an oxygen desorption peak which shifted, starting from 700 K, to higher temperatures up to 900 K with increasing adsorption temperature. The intensity of this peak did not saturate, and therefore it was assigned to oxygen dissolved in the bulk of (polycrystalline) silver. This assignment has been criticized by Herein et al. [He96], but a similar peakshift has been reported by these authors for that peak, which they identified with bulk oxygen. Thus, there is a striking resemblance between O/Ag and O/Au concerning the TD behaviour: Increasing the temperature during oxygen exposure to Ag has a similar effect on the bulk oxygen TD peaks as increasing the ion energy during sputtering of O^+ ions onto Au(110) (see Fig. 7.1). Apart from the shift of the desorption maximum to higher temperatures for elevated dosing temperatures, the leading edges of the O/Ag spectra cross as well. Rehren et al. [Re91] regarded this behaviour as typical for a bulk-dissolved species. Obviously, a higher dosing temperature leads to an enhanced mobility of the oxygen atoms in the silver lattice and thus allows the occupation of sites located deeper inside the bulk. Increasing the ion energy during sputter deposition of oxygen has clearly the same effect. These similarities between the TD peaks of dissolved oxygen in silver and sputtered oxygen in gold support our idea that the γ_4 state corresponds to oxygen atoms dissolved in bulk gold. Continuing the comparison we note that the on-surface state γ_2 on Au has its counterpart in the Ag-O_α state. However, we

found no analogon to Ag-O_γ, i.e., there no clear evidence for the existence of strongly bound 'surface embedded' chemisorbed oxygen on gold, although previous STM, REM, and RHEED investigations suggested the formation of such a species by exposure of an Au(111) surface to O_2 at atmospheric pressure and high temperature (1070 K) [Hu95, Ch96, Hu96, Uc98]. As a speculation, the small shoulder around 900 K on the high-temperature side of the spectra (b) and (c) in Fig. 7.1 and the positive $\Delta\varphi$ value above 800 K may be regarded as hints for a similar strongly interacting oxygen species on Au(110).

(iii) COMPARISON OF OXYGEN PHASES OBTAINED BY SPUTTERING WITH THOSE FORMED THROUGH ELECTRON BOMBARDMENT – Chemisorbed oxygen (β_2) and surface gold oxide (β_1), desorbing around 550 K and 490 K, respectively, can easily be produced by electron bombardment of physisorbed oxygen at 28 K (see Chapter 6). This technique, which involves the intermediate formation of oxygen atoms, does, however, not lead to the formation of subsurface or bulk species, as the absence of a high-temperature desorption state like γ_4 reveals.

	E_{des} [kJ/mol]	ν [s^{-1}]
β_1	131	3×10^{13}
β_2	147	6×10^{12}
γ_1	103	5.3×10^{11}
γ_2	158	8.5×10^{13}

Table 7.2: Comparison of the present data with desorption activation parameters for gold oxide (β_1) and chemisorbed oxygen atoms (β_2) prepared by electron bombardment of physisorbed oxygen at 28 K. Values for the β states were taken from Section 6.1.

The desorption activation parameters obtained for the species γ_1 and γ_2 can be compared with the respective values for surface gold oxide and chemisorbed oxygen. The respective data, also evaluated by analysis of a heating rate variation (see Section 6.1), are presented in Table 7.2. The desorption energy of surface gold oxide (β_1 state) is significantly higher than that for the γ_1 state, whereas the γ_2 state has a slightly higher desorption energy than chemisorbed oxygen (β_2). Similar deviations can be seen among the frequency factors of the respective β and γ states. Furthermore, both β and γ states exhibit a similarly high reactivity towards carbon monoxide, a behaviour which suggests that they correspond to

oxygen species located on the surface or in the subsurface range. As a major difference, desorption of β_1 has only a small influence on the work function (see Section 6.5), in contrast to γ_1 (see Section 7.3). Clearly, the *surface-near* oxygen phases formed by electron bombardment of physisorbed oxygen and by oxygen ion sputtering are similar, although not identical.

(iv) EFFICIENCY OF OXYGEN DEPOSITION BY SPUTTERING – The flux of ions becoming neutralized at the gold surface is nicely reflected in the current density measured between sample and ground during sputtering. However, possible competitive processes prevent us from establishing a simple relationship between current density and flux of ions finally deposited inside the material. Nevertheless, one can estimate an *upper limit for the ion flux*, since all secondary phenomena (e.g., secondary electron emission, ion neutralization without implantation, removal of deposited oxygen by sputtering) and other systematic errors (e.g., sputtering of the sample holder) always enhance the (positive) sample current and therefore lead to an overestimation of the ion flux. If we further assume that the measured current is completely caused by O_2^+ (rather than by O^+) ions, we are able to give an upper limit for the *flux of reactive oxygen species* onto the surface. Through comparison with actual coverages; this value will enable us to derive then a lower limit for the *efficiency of oxygen deposition* by ion sputtering.

According to the given assumptions, a sample current density of 2.0 μA/cm^2 corresponds to a deposition rate of 2.5×10^{13} oxygen *atoms* per cm^2 per second, equivalent to 0.015 ML/s. (For the definition of the monolayer see above.) For example, 20 minutes sputtering at 2.0 μA/cm^2 (as for spectrum (b) in Fig. 7.5) should lead to an oxygen coverage equal or less than 18 ML. The measured value is 18.5 ML. Therefore, within the margin of error of the coverage measurement (< 20 %), the efficiency Y of the sputtering deposition, defined as the number of deposited atoms divided by the number of atoms contained in the neutralized ions, is $Y \approx 1$ for the given example.

However, a certain fraction of the ions impinging on the surface is not neutralized. In low-energy ion scattering (LEIS) experiments often a neutralization probability around 90 % is observed (for He^+ at an ion energy of 1 keV) [Ni93], which means that roughly 10 % of the ions are additionally lost through scattering processes, if the neutralization probability is similar in our case.

(v) THE γ_3 DESORPTION STATE – The desorption state γ_3 has a remarkable property: it does not shift when the heating rate is varied. Since the Polanyi-Wigner equation (Eq. 4.1) and, therefore, Eq. 4.11 apply to *any* activated process, we should expect a peak shift not only if the desorption itself is rate-limiting, but also for a diffusion-controlled desorption or for any other activated process. A kinetically controlled desorption process can therefore be excluded in the case of γ_3. However, close to the

desorption temperature of γ_3 the (1×2)-'missing row' structure of Au(110) undergoes an order-disorder transition with a critical temperature of 650 K [Cl86]. The beginning of this process could open up channels for the desorption of this oxygen species.

Notably, a desorption peak that is independent of the heating rate has also been observed on the oxygen-silver (polycrystalline) system by Herein et al. [He96]. The authors proposed that a continuous change between various different rate-limiting steps is responsible for that behaviour.